Tight-binding model for semiconductor nanostructures

S. Schulz and G. Czycholl
Institute for Theoretical Physics, University of Bremen, D-28334 Bremen, Germany
(Received 26 January 2005; revised manuscript received 4 May 2005; published 14 October 2005)

An empirical $s_c p_a^3$ tight-binding (TB) model is applied to the investigation of electronic states in semiconductor quantum dots. A basis set of three p orbitals at the anions and one s orbital at the cations is chosen. Matrix elements up to the second nearest neighbors and the spin-orbit coupling are included in our TB model. The parametrization is chosen so that the effective masses, the spin-orbit splitting and the gap energy of the bulk CdSe and ZnSe are reproduced. Within this reduced $s_c p_a^3$ TB basis the valence (p) bands are excellently reproduced and the conduction (s) band is well reproduced close to the Γ point, i.e., near to the band gap. In terms of this model much larger systems can be described than within a (more realistic) sp^3s^* basis. The quantum dot is modeled by using the (bulk) TB parameters for the particular material at those sites occupied by atoms of this material. Within this TB model we study pyramidal-shaped CdSe quantum dots embedded in a ZnSe matrix and free spherical CdSe quantum dots (nanocrystals). Strain effects are included by using an appropriate model strain field. Within the TB model, the strain effects can be artificially switched off to investigate the influence of strain on the bound electronic states and, in particular, their spatial orientation. The theoretical results for spherical nanocrystals are compared with data from tunneling spectroscopy and optical experiments. Furthermore the influence of the spin-orbit coupling is investigated.

DOI: 10.1103/PhysRevB.72.165317 PACS number(s): 73.22.Dj, 68.65.Hb, 71.15.Ap

I. INTRODUCTION

Semiconductor quantum dots[1,2] (QDs) are of particular interest, both concerning basic research and possible applications. QDs are considered to be zero-dimensional objects, i.e., systems confined in all three directions of space with a typical size of the magnitude of several nanometers. Therefore, these systems are realizations of "artificial atoms" whose form and size can be manipulated. Concerning basic research these nanostructures (QDs) are interesting, as the methods of quantum theory can be applied to systems on new scales and with new symmetries in between that of atoms or molecules and of macroscopic crystals. On the other side light emission and absorption just from the localized states in such devices may be important for optoelectronic applications,[3,4] quantum cryptography,[5] and quantum computing.[6]

Semiconductor QDs can be realized by means of metallic gates providing external (electrostatic) confinement potentials,[7] by means of self-organized clustering of certain atoms in the Stranski-Krastanow (SK) growth mode[8–10] or chemically by stopping the crystallographic growth using suitable surfactant materials.[11–14] Here we deal only with the latter two types of QDs. The QDs created in the SK growth mode emerge self-assembled or self-organized in the epitaxial growth process because of the preferential deposition of material in regions of intrinsic strain or along certain crystallographic directions. In epitaxial growth of a semiconductor material A on top of a semiconductor material B only one or a few monolayers of A material may be deposited homogeneously as a quasi-two-dimensional A layer on top of the B surface forming the so-called wetting layer (WL). Under certain conditions and for certain materials further deposited A atoms will not form a further homogeneous layer but they will cluster and form islands of the A material because this may lower the elastic energy due to the lattice mismatch of the A and B material. If one then stops the growth process, one has free A QDs on top of an A WL on the B material. If one continues the epitaxial growth process with B material, one obtains embedded quantum dots (EQDs), i.e., QDs of the A material on top of an A-WL embedded within B material.

The chemically realized QDs emerge by means of colloidal chemical synthesis.[11,12] Thereby the crystal growth of the semiconductor material in the surrounding of soaplike films called surfactants is stopped when the surface is covered by a monolayer of surfactant material. Thus one obtains tiny crystallites of the nanometer size in all three directions of space; this is why these QDs are also called "nanocrystals" (NCs). The size and the shape of the grown NCs can be controlled by external parameters such as growth time, temperature, concentration, and surfactant material.[13,14] Certain physical properties such as the band gap (and thus the color) depend crucially on the size of the NCs. Typical diameters for both, EQDs and NCs, are between 3 and 30 nm, i.e., they contain between 10^3 up to 10^5 atoms. Therefore, EQDs and NCs can be considered to be a new, artificial kind of condensed matter in between molecules and solids. For the in SK-modus grown EQDs lens-shaped dots,[15] dome shaped and pyramidal dots,[8,16,17] and also truncated cones[18] have been found and considered.

Of course the fundamental task is the calculation of the electronic properties of EQDs and NCs. But here one encounters the difficulty that these systems are much larger than conventional molecules and that the fundamental symmetry of solid state physics, namely translational invariance, is not fulfilled. Therefore, neither the standard methods of theoretical chemistry nor the ones of solid state theory can immediately be applied to systems with up to 10^5 atoms. Conventional *ab initio* methods of solid state theory based on density functional theory (DFT) and local density approximation (LDA) would require supercell calculations. But the size of the supercell must be larger than the EQD or NC, and

such large supercells are still beyond the possibility of present day computational equipment. Therefore, only systems with up to a few hundred atoms can be investigated in the framework of the standard *ab initio* DFT methods.[19–21] Simple model studies based on the effective mass approximation[15,22] or a multiband $\vec{k}\cdot\vec{p}$ model[23–25] describe the QD by a confinement potential caused by the band offsets, for instance, they give qualitative insights into the formation of bound (hole and electron) states, but they are too crude for quantitative, material specific results or predictions. More suitable for a microscopic description are empirical pseudopotential methods[26–29] as well as empirical tight-binding models.[30–41] The empirical pseudopotential methods allow for a detailed variation of the wave functions on the atomic scale. This is certainly the most accurate description from a microscopic, atomistic view point, but it requires a large set of basis states. Within a TB model some kind of coarse graining is made and one studies spatial variations only on interatomic scales and no longer within one unit cell. The advantage is that usually a small basis set is sufficient, which allows for the possibility to study larger systems. Furthermore the TB model provides a simple physical picture in terms of the atomic orbitals and on-site and inter-site matrix elements between these orbitals. A cutoff after a few neighbor shells is usually justified for orbitals localized at the atomic sites.

Semiempirical TB models have been used already to describe "nearly" spherical InAs and CdSe NCs for which the dangling bonds at the surfaces are saturated by hydrogen[31–34] or organic ligands.[37–39] Also uncapped[42] and capped[35] pyramidal InAs QDs were investigated by use of an empirical TB model. In the latter work an sp^3s^* basis was used leading to a $10N\times 10N$ Hamiltonian matrix, where N is the number of atoms, with 33 independent parameters. In the present paper we apply a similar TB model to II-VI nanostructures, namely, CdSe EQDs embedded within ZnSe and spherical CdSe NCs. We show that a smaller TB basis is sufficient, namely an $s_cp_a^3$ basis, i.e., four states per unit cell and spin direction. This requires only 8 independent parameters and, in principle, this allows for the investigation of larger nanostructures than those accessible in Ref. 35. Strictly speaking, the $s_cp_a^3$ basis set leads to a smaller matrix dimension and also to a smaller number of nonzero matrix elements compared to the sp^3s^* TB model. So the $s_cp_a^3$ TB model is numerically less demanding regarding both memory requirements and computational time. For the bulk system the valence p bands are excellently reproduced and the conduction s band is well reproduced close to the Γ point. Therefore, we expect that also for the QDs all the hole states and at least the lowest lying electron states (close to the gap) are well reproduced. We investigate, in particular, the influence of strain effects on the electronic structure. To examine the accuracy of our model we compare the results to other microscopic and macroscopic models. Furthermore, TB results for CdSe-NCs are compared to experimental results, and a very good agreement is obtained; for instance, for the dependence of the energy gap the NC diameter. This demonstrates that our TB model with a reduced basis set is reliable and sufficient for the reproduction of the most essential electronic properties of the nanostructures.

This work is organized as follows. In Sec. II our TB model is presented. The formalism of how to obtain the TB parameters and how to apply them to the description of EQDs and NCs is described. In Sec. III the inclusion of strain effects in our model is introduced. Results for the pyramidal CdSe EQDs are presented. For the spherical CdSe NCs the results and the comparison with the experimental data are presented in Sec. IV. Section V contains a summary and a conclusion.

II. THEORY

A. TB model for bulk materials

In this work we use a TB model with eight basis states per unit cell. Such a model has been successfully used for the investigation of optical properties in ZnSe quantum wells.[46] For the description of the bulk semiconductor compounds CdSe and ZnSe we choose an $s_cp_a^3$ basis set. That implies that the set of basis states $|\nu,\alpha,\sigma,\vec{R}\rangle$ is given by four orbitals $\alpha=s,p_x,p_y,p_z$ with spin $\sigma=\pm\frac{1}{2}$. One s orbital at the cation ($\nu=c$) and three p orbitals at the anion ($\nu=a$) site in each unit cell $\vec{R}$ are chosen. The TB matrix elements are given by

$$E_{\alpha,\alpha'}(\vec{R}'-\vec{R})_{\nu,\nu'}=\langle\nu',\alpha',\sigma'\vec{R}'|H^{\text{bulk}}|\nu,\alpha,\sigma,\vec{R}\rangle. \quad (1)$$

The coupling of the basis orbitals is limited to nearest and next nearest neighbors. Following Ref. 47, the spin-orbit component of the bulk Hamiltonian H^{bulk} couples only p orbitals at the same atom. With the two center approximation of Slater and Koster[48] we are left with only eight independent matrix elements $E_{\alpha,\alpha'}(\vec{R}'-\vec{R})_{\nu,\nu'}$.

In $\vec{k}$ space, with the basis states $|\vec{k},\nu,\alpha,\sigma\rangle$, the electronic properties of the pure bulk material are modeled by an 8×8 matrix $\mathbf{H}^{\text{bulk}}(\vec{k})$ (for each $\vec{k}$ from the first Brillouin zone). This matrix depends on the different TB parameters $E_{\alpha,\alpha'}(\vec{R}'-\vec{R})_{\nu,\nu'}$. By analytical diagonalization for special $\vec{k}$ directions, the electronic dispersion $E_n(\vec{k})$ is obtained as a function of the TB parameters; here n is the band index. Equations for the different TB parameters $E_{\alpha,\alpha'}(\vec{R}'-\vec{R})_{\nu,\nu'}$ can now be deduced as a function of the Kohn-Luttinger-parameters $(\gamma_1,\gamma_2,\gamma_3)$, the energy gap E_{gap}, the effective electron mass m_e, and the spin-orbit-splitting Δ_{so}. The zero level of the energy scale is fixed to the valence-band maximum. The used material parameters for CdSe and ZnSe are given in Table I. The resulting numerical values for the different TB parameters (obtained by optimizing them so that the resulting TB band structure reproduces the parameters given in Table I) are summarized in Table II (with and without taking into account a site-diagonal parameter for the spin-orbit coupling). Within this approach, the characteristic properties of the band structure in the region of the Γ point are well reproduced, as can be seen from Fig. 1, which shows the TB bands of bulk CdSe and ZnSe (using the TB parameters with spin-orbit coupling). When comparing with band-structure results from the literature,[49] one sees that the three valence (p) bands are excellently reproduced whereas the s-like conduction band is well reproduced only close to the Γ

TABLE I. Properties of the CdSe and ZnSe band structures. The lattice constants are given by 6.077 and 5.668 Å, respectively. E_g denotes the band gap, Δ_{so} the spin-orbit coupling, and m_e the effective electron mass. The Kohn-Luttinger-parameters are γ_1, γ_2, and γ_3. The C_{ij} are the elements of the elastic stiffness tensor.

	CdSe	ZnSe
E_g (eV)	1.74 (Ref. 43)	2.8201 (Ref. 43)
Δ_{so} (eV)	0.41 (Ref. 43)	0.43 (Ref. 43)
m_e	0.12 (Ref. 43)	0.147 (Ref. 44)
γ_1	3.33 (Ref. 43)	2.45 (Ref. 44)
γ_2	1.11 (Ref. 43)	0.61 (Ref. 44)
γ_3	1.45 (Ref. 43)	1.11 (Ref. 44)
C_{12} (GPa)	46.3 (Ref. 45)	50.6 (Ref. 45)
C_{11} (GPa)	66.7 (Ref. 45)	85.9 (Ref. 45)

point. This is understandable, because higher (unoccupied) conduction bands are neglected, and can be improved by taking into account more basis states per unit cell. But for a reproduction of the electronic properties in the region near the Γ point, which is important for a proper description of the optical properties of the semiconductor materials, the $s_c p_a^3$ TB model is certainly sufficient and satisfactory.

B. TB model for embedded quantum dots and nanocrystals

Having determined suitable TB parameters for the bulk materials (here CdSe and ZnSe) a EQD or NC can be modeled simply by using the TB parameters of the bulk materials for those sites (or unit cells) occupied by atoms (or molecules) of this material. Concerning the on-site matrix elements this condition is unambiguous. Concerning the intersite matrix elements one also uses the bulk matrix elements, if the two sites are occupied by the same kind of material, but one has to use suitable averages of the bulk intersite matrix elements for matrix elements over interfaces between different material, i.e., if the two sites (or unit cells) are occupied by different atoms (or molecules). Concerning the surfaces or boundaries of the nanostructure there are different possibilities. One can use fixed boundary conditions, i.e., effectively use zero for the hopping matrix elements from a surface atom to its fictitious nearest neighbors, or (for the embedded QDs) one can use periodic boundary conditions to avoid any surface effects, which artificially arise from the finite cell size used for the EQD modeling. For the NCs the best thing to do is a realistic, atomistic modeling of the organic ligands covering the NC surface, as described in Refs. 39, 50, and 51. Within the restricted basis set thus selected the ansatz for an electronic eigenstate of the EQD or NC is, of course, a linear combination of the atomic orbitals $|\nu,\alpha,\sigma,\vec{R}\rangle$:

$$|\Phi\rangle = \sum_{\alpha,\nu,\sigma,\vec{R}} u_{\nu,\alpha,\sigma,\vec{R}} |\nu,\alpha,\sigma,\vec{R}\rangle. \quad (2)$$

Here $\vec{R}$ denotes the unit cell, α the orbital type, σ the spin, and ν an anion or cation. Then the Schrödinger equation leads to the following finite matrix eigenvalue problem:

TABLE II. TB parameters (in eV) with (TB) and without (TB-NO SO) spin-orbit coupling for ZnSe and CdSe, using the notation of Ref. 48.

Material	Parameter	TB	TB-NO SO
ZnSe	$E_{xx}(000)_{aa}$	−1.7277	−2.0413
	$E_{ss}(000)_{cc}$	7.0462	12.1223
	$E_{sx}(\frac{1}{2}\frac{1}{2}\frac{1}{2})_{ac}$	1.1581	0.2990
	$E_{xx}(110)_{aa}$	0.1044	0.2185
	$E_{xx}(011)_{aa}$	0.1874	0.0732
	$E_{xy}(110)_{aa}$	0.3143	0.4285
	$E_{ss}(110)_{cc}$	−0.3522	−0.7752
	λ	0.1433	0
CdSe	$E_{xx}(000)_{aa}$	−1.2738	−1.7805
	$E_{ss}(000)_{cc}$	3.6697	10.8053
	$E_{sx}(\frac{1}{2}\frac{1}{2}\frac{1}{2})_{ac}$	1.1396	0.4260
	$E_{xx}(110)_{aa}$	0.0552	0.2161
	$E_{xx}(011)_{aa}$	0.1738	0.0129
	$E_{xy}(110)_{aa}$	0.1512	0.3120
	$E_{ss}(110)_{cc}$	−0.1608	−0.7554
	λ	0.1367	0

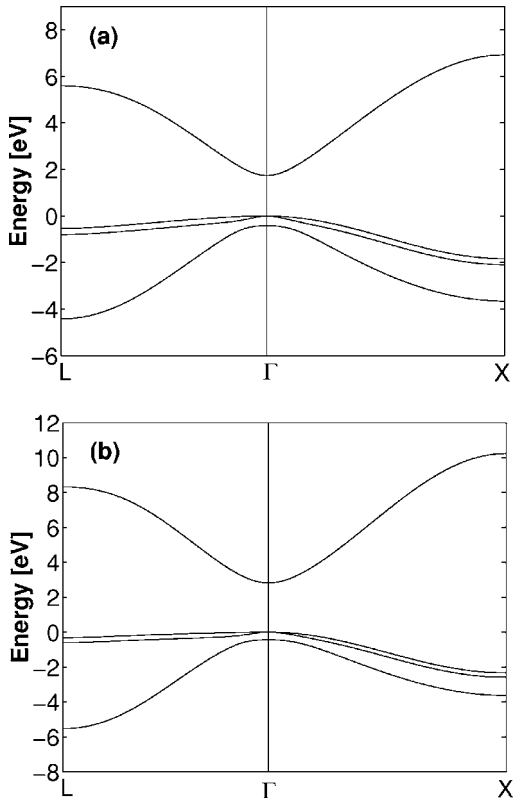

FIG. 1. Tight-binding band structures for CdSe (a) and ZnSe (b).

$$\sum_{\alpha,\nu,\sigma,\vec{R}} \langle \nu',\alpha',\sigma',\vec{R}'|H|\nu,\alpha,\sigma,\vec{R}\rangle u_{\nu,\alpha,\sigma,\vec{R}} - E u_{\nu',\alpha',\sigma',\vec{R}'} = 0, \tag{3}$$

where E is the energy eigenvalue. The shortcut notation $\langle \nu',\alpha',\sigma',\vec{R}'|H|\nu,\alpha,\sigma,\vec{R}\rangle = H_{l\vec{R}',m\vec{R}}$ is used in the following for the matrix elements with $l=\nu',\alpha',\sigma'$ and $m=\nu,\alpha,\sigma$.

The matrix elements for CdSe and ZnSe without strain are denoted by $H^0_{l\vec{R}',m\vec{R}}$. For these matrix elements the TB parameters $E_{\alpha,\alpha'}(\vec{R}'-\vec{R})_{\nu,\nu'}$ of the bulk materials, determined in Sec. II A, are used. For the off-diagonal matrix elements over interfaces and the diagonal matrix elements of the selen atoms at the interface between dot and barrier, which do not unambiguously belong to the ZnSe or CdSe, respectively, we choose the mean value of the parameters for the two materials. Furthermore, a parameter for the valence-band offset ΔE_V has to be included in the model. This means that for CdSe in a heterostructure, i.e., surrounded by a barrier ZnSe material, all diagonal matrix elements are shifted just by ΔE_V compared to the bulk CdSe diagonal matrix elements. In the literature different values for ΔE_V can be found, they vary in the range of 10–30 % of the band gap difference between CdSe and ZnSe.[9,52,53] We have performed calculations with valence-band offsets of $\Delta E_V=0.108$ eV, $\Delta E_V=0.22$ eV, and $\Delta E_V=0.324$ eV, which corresponds to 10%, 20%, and 30% of the difference of the band gaps. We find that these different choices for ΔE_V shift the EQD energy gap $E^{\mathrm{QD}}_{\mathrm{gap}}$ by less than 2%. This shows that the results are not much affected by the specific choice of the valence-band offset ΔE_V. Therefore, in the following, an intermediate value of $\Delta E_V = 0.22$ eV is chosen.

Furthermore, in a heterostructure of two materials with different lattice constants, strain effects have to be included for a realistic description of the electronic states, because the distance between two CdSe unit cells and the bond angles are not the same as the corresponding equilibrium values in bulk CdSe. This means that the TB matrix elements $H_{l\vec{R}',m\vec{R}}$ in the EQD differ from the $H^0_{l\vec{R}',m\vec{R}}$ matrix elements in the bulk material. Though a scaling of the on-site matrix elements may also be important, as discussed in Refs. 55 and 54 we will assume only scaling of the intersite matrix elements, for which, in general, a relation

$$H_{l\vec{R}',m\vec{R}} = H^0_{l\vec{R}',m\vec{R}} f(\vec{d}^0_{\vec{R}'-\vec{R}}, \vec{d}_{\vec{R}'-\vec{R}}) \tag{4}$$

has to be expected, where $\vec{d}^0_{\vec{R}'-\vec{R}}$ and $\vec{d}_{\vec{R}'-\vec{R}}$ are the bond vectors between the atomic positions of the unstrained and strained material, respectively. The function $f(\vec{d}^0,\vec{d})$ describes, in general, the influence of the bond length and the bond angle on the intersite (hopping) matrix elements. For lack of a microscopic theory for the functional form we use as a simplified model assumption $f(\vec{d}^0_{\vec{R}'-\vec{R}}, \vec{d}_{\vec{R}'-\vec{R}}) = (d^0_{\vec{R}'-\vec{R}}/d_{\vec{R}'-\vec{R}})^2$. With this d^{-2} ansatz, the interatomic matrix elements $H_{l\vec{R}',m\vec{R}}$, with $\vec{R}' \neq \vec{R}$, are given by

$$H_{l\vec{R}',m\vec{R}} = H^0_{l\vec{R}',m\vec{R}} \left(\frac{d^0_{\vec{R}'-\vec{R}}}{d_{\vec{R}'-\vec{R}}} \right)^2. \tag{5}$$

This corresponds to Harrison's[56] d^{-2} rule, the validity of which has been demonstrated for II-VI materials and nearest neighbors by Sapra *et al.*[57] We use this power-law scaling also for the second nearest neighbors, which may be considered to be simply a best guess, because the scaling of more distant matrix elements is not nearly as well understood as that of nearest neighbor matrix elements. More sophisticated ways to treat the scaling of the interatomic matrix elements, e.g., by calculating the dependence of energy bands on volume effects and different exponents for different orbitals, can be found in the literature.[35,41,55] Furthermore the results of Bertho *et al.*[58] for the calculations of hydrostatic and uniaxial deformation potentials in the case of ZnSe show that the d^{-2} rule should be a reasonable approximation. Our model assumption for the function $f(\vec{d}^0,\vec{d})$ means that we neglect the influence of bond angle distortion. Though energy shifts due to bond angle distortions have been found for InAs EQDs,[35] here the negligence of bond angle distortion can be justified when exclusively taking into account the coupling between *s*, and *p*, orbitals at nearest neighbor sites. Piezoelectric fields, which are usually considered to be less important for the zinc blende structures realized in CdSe and ZnSe,[24] are also not taken into account in our model.

The problem is now reduced to the diagonalization of a finite but very large matrix. To calculate the eigenvalues of this matrix, in particular, the bound electronic states in the QD, the folded spectrum method[59] is applied to the eigenvalue problem of Eq. (3).

III. RESULTS FOR A PYRAMIDAL CdSe EMBEDDED QUANTUM DOT

A. Geometry and strain

To model a CdSe QD embedded into a ZnSe barrier material we choose a finite (zinc blende) lattice within a box with fixed boundary conditions. Within this box we consider a CdSe WL of thickness $1a$ (lattice constant of the conventional unit cell, i.e. about two anion and two cation layers), and on top of this wetting layer there is a pyramidal QD with base length b and height $h=b/2$. For the matrix elements corresponding to sites within the WL or the QD we choose the TB values appropriate for CdSe, for all other sites within the box for ZnSe. Figure 2 shows a schematic picture of this geometry we use to model the EQD. We investigate EQDs with a base length b of $6a$, $8a$, and $10a$, where $a=5.668$ Å is the lattice constant of the bulk ZnSe material. Cells with the dimensions of $18a\times18a\times15a$ (38 880 atoms), $20a\times20a\times16a$ (51 200 atoms), and $22a\times22a\times17a$ (65 824 atoms) are used for the calculations. Figure 2 shows the EQD with a base length b of $10a$. Fixed boundary conditions are applied to avoid a dot-dot coupling in contrast to periodic boundary conditions.[35] The total size of the cells is chosen so that the boundary conditions affect the energy gap of the EQD by less than 2%.

To consider strain effects in our model the knowledge of the strain tensor $\boldsymbol{\epsilon}$ is necessary. The strain tensor $\boldsymbol{\epsilon}$ is related

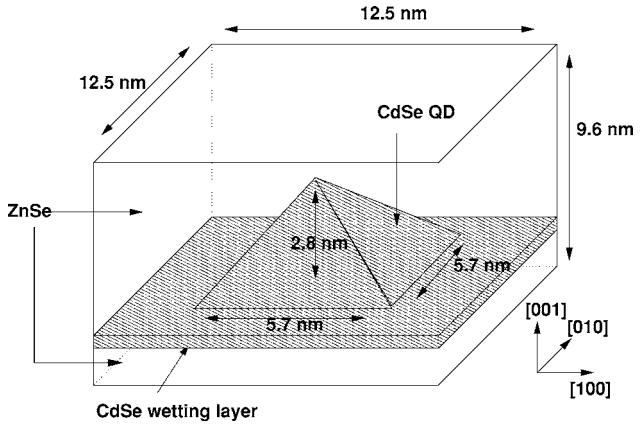

FIG. 2. Schematic visualization of the pyramidal CdSe QD buried in a ZnSe matrix. The wetting layer has a thickness of one lattice constant ($1a$) of bulk ZnSe. The pyramidal QD has a base length b of ten times the ZnSe lattice constant ($b=10a$).

to the strain dependent relative atomic positions $\vec{d}_{\vec{R}'-\vec{R}}$ by

$$\vec{d}_{\vec{R}'-\vec{R}} = (\mathbb{1} + \boldsymbol{\epsilon})\vec{d}^{\,0}_{\vec{R}'-\vec{R}}. \tag{6}$$

To appoint the strain tensor outside the EQD, the WL is treated as a quantum film. In the absence of a shear strain ($\epsilon_{i,j} \sim \delta_{i,j}$) for a coherently grown film, the strain components are given by[60]

$$\epsilon_{\parallel} = \epsilon_{xx} = \epsilon_{yy} = \frac{a_S - a_D}{a_D}, \tag{7}$$

$$\epsilon_{\perp} = \epsilon_{zz} = -\frac{C_{12}}{C_{11}}\epsilon_{\parallel}. \tag{8}$$

Here a_D is the lattice constant of the unstrained film material and a_S denotes the parallel lattice constant of the substrate. In Table I the cubic elastic constants C_{ij} of the bulk materials are given. The resulting strain profile for a line scan in the z direction outside the dot is shown in Fig. 3(a). In Ref. 23 Stier *et al.* considered a similar strain profile for an InAs/GaAs EQD. The lattice mismatch of approximately 7% in the InAs/GaAs system is nearly the same as for the CdSe/ZnSe system. So our calculated strain profile shows the same behavior as the profile in Ref. 23 for a line scan in the z direction outside the EQD.

To obtain the strain profile inside the EQD we use a model strain profile, which shows a similar behavior as the strain profiles which are given in Refs. 23 and 61 for a line scan in the z direction through the tip of the pyramid. This model strain profile is displayed in Fig. 3(b). The shear components, ϵ_{xy}, ϵ_{xz}, and ϵ_{yz}, can be neglected, at least away from the boundaries of the dot.[22]

B. Bound single particle states

We have calculated the first five states for electrons and holes for three different EQD sizes. These calculations are done with and without including strain effects. For the evaluations without strain we have chosen the exponent in Eq. (5)

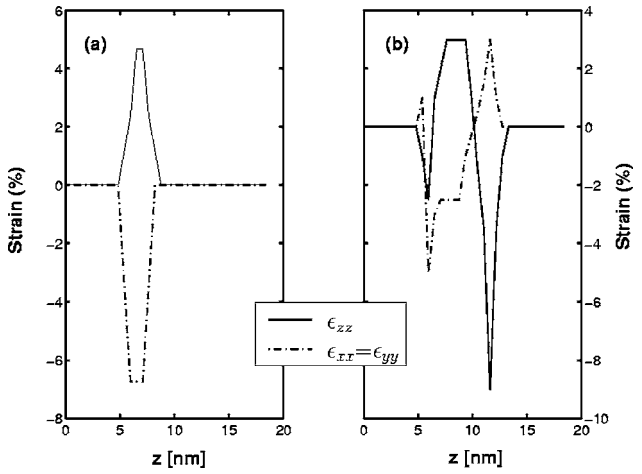

FIG. 3. Strain distribution in and around the embedded pyramidal CdSe QD with a base length of $b=10a$. The WL at the base of the QD is $1a$ thick. The whole structure is buried in a ZnSe matrix. Line scans along the [001] direction through the WL outside the dot (a) and inside the dot through the tip of the pyramid (b) are displayed. The diagonal elements of the strain tensor $\boldsymbol{\epsilon}$ are shown as solid (ϵ_{zz}) and dashed-dotted lines ($\epsilon_{xx}=\epsilon_{yy}$).

to be zero. The energy spectrum obtained from these calculations is shown in Fig. 4(a) without strain and in Fig. 4(b) including strain effects. The states are labeled by e_1 and h_1 for electron and hole ground states, e_2 and h_2 for the first excited states, and so on. All energies are measured relative to the valence-band maximum of ZnSe. Figure 4 also shows the size dependence of the electron and hole energy levels. The energies are compared with the ground state energies for electrons and holes in the $1a$ thick CdSe WL (WL_{e_1} and WL_{h_1}, respectively), which is calculated separately for a coherently strained quantum film (i.e., the WL without the QD). As expected from a naive particle in a box picture, the

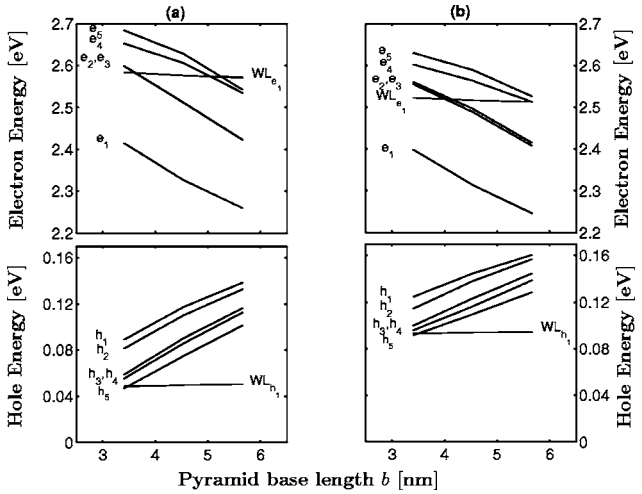

FIG. 4. Electron and hole energies for embedded pyramidal CdSe/ZnSe QDs on a WL of thickness $1a$ (roughly 4 ML) for different base lengths of the dot without strain (a) and with strain effects taken in to account (b). The ground state energies for electrons (WL_{e_1}) and holes (WL_{h_1}) for the WL (of thickness $1a$) alone are also displayed.

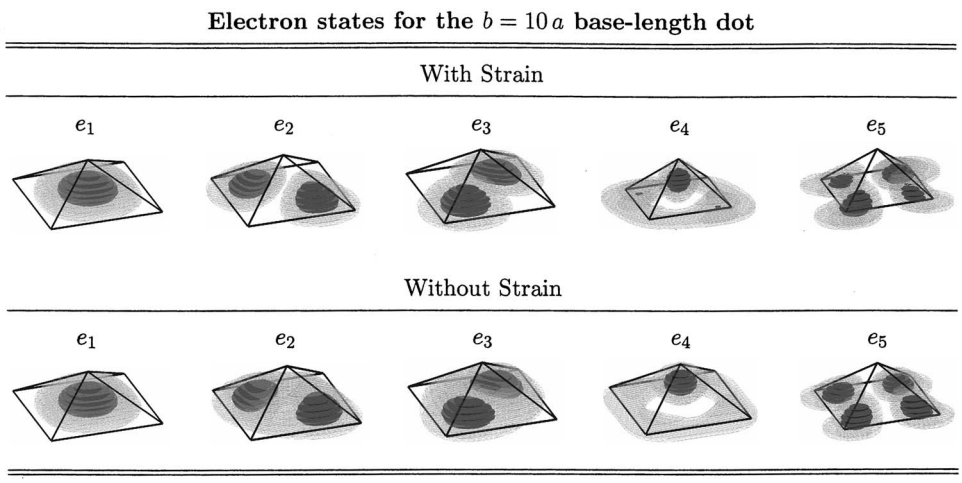

FIG. 5. Isosurfaces of the squared electron wave functions with and without strain for the embedded $b=10a$ pyramidal QD. The light and dark surfaces correspond to 0.1 and 0.5 of the maximum probability density, respectively.

binding of electrons and holes becomes stronger in the EQD when the dot size is increased. The quantum confinement causes the number of bound states to decrease when the dot size is reduced. For the EQDs with a base length $b=8a$ and $b=10a$ the calculated hole states are well above the WL energy (WL_{h_1}). This is valid for the strain-unaffected and strained EQD. For the system with $b=6a$ we obtain at least four bound hole states in both models. The energy splitting between the different states is only slightly influenced by the strain. Furthermore we see from Fig. 4 that the number of bound electron states is influenced by the strain. For the system with a base length of $b=10a$ we get at least three bound-electron states when we take strain effects into account [Fig. 4(b)]. Without strain effects at least five bound states are found. So the confinement potential for the electrons is effectively reduced by the strain.

The bound electron states e_2 and e_3 are energetically not degenerate even without strain. This arises from the C_{2v} symmetry of the system. Already from the geometry of the EQD system it is clear that there is no (001) mirror plane. Furthermore, if one considers a (001) plane with sites occupied by Se anions, the nearest neighbor (cation) planes in the $\pm z$ direction are not equivalent, as for the zinc blende structure the nearest neighbors above the plane are found in the $[111]$ direction and below the plane in the $[1\bar{1}\bar{1}]$ direction. So also for crystallographic reasons a (001) plane is not a mirror plane. Finally, if one considers the base plane of the EQD (or the WL) to be this anion (001) plane, there are different cations, namely Cd above and Zn below this plane. Therefore, the QD system has reduced C_{2v} symmetry. In theories based on continuum models, e.g., effective mass approximations,[15,22] the discussed effects cannot be accounted for. These interfacial effects also affect the one-particle wave functions in the system. In Fig. 5 the isosurfaces for the squared electron wave functions $|\Phi_i(\vec{r})|^2$ are displayed with and without strain, respectively. The light and dark isosurface levels are selected as 0.1 and 0.5 of the maximum probability density, respectively. For both calculations, the lowest electron state e_1 is an s-like state according to its nodal structure. The next two states e_2 and e_3 are p-like states. These states are oriented along the $[1\bar{1}0]$ and the $[110]$ direction, respectively. Due to the different atomic structure along these directions we find a p-state splitting $\Delta^0_{e_2,e_3}=E_{e_3}-E_{e_2}$ for the unstrained EQD of about 0.43 meV. In conventional $\vec{k}\cdot\vec{p}$ models[22,25] an unstrained, square-based pyramidal EQD is modeled with a C_{4v} symmetry. In our microscopic model the resulting degeneracy is lifted and a splitting occurs as a consequence of the reduction of C_{4v} symmetry to a C_{2v} zinc blende symmetry.

The strain splits the states e_2 and e_3 further. Due to the different atomic structure, the strain profile within each plane (perpendicular to the growth z direction) along the $[110]$ and $[1\bar{1}0]$ direction is different.[61] This effect contributes also to the anisotropy. Due to the fact that the base is larger than the top, there is a gradient in the strain tensor between the top and the bottom of the pyramid. In the EQD, the cation neighbors above each anion are found in the $[111]$ direction while the cation neighbors below are found in the $[1\bar{1}\bar{1}]$ direction. Therefore, the cations along the $[1\bar{1}0]$ direction are systematically more stressed than the cations along the $[110]$ direction. In the case of strain we find a p-state splitting of $\Delta^{\text{strain}}_{e_2,e_3}=7.1$ meV. Compared to the states e_2 and e_3 of the unstrained EQD, the two lumps of the light isosurfaces are well separated. The states e_2 and e_3 reveal nodal planes along the $[110]$ and $[1\bar{1}0]$ directions, respectively.

The state e_4 for the strained dot is resonant with a WL state, so the wave function is leaking into the WL. Also the wave function of the state e_5 is localized at the base of the pyramid but clearly shows already a finite probability density inside the WL. The states e_4 and e_5 of the unstrained EQD are still mainly localized inside the dot. The classification of the state e_4 by its nodal structure is difficult. e_4 is similar to a p state which is oriented along the $[001]$ direction. The electron state e_5 is d like.

Figure 6 shows the isosurface plots of the squared wave function $|\Phi_i(\vec{r})|^2$ for the lowest five hole states h_1-h_5 with and without strain. The light and dark isosurface levels are again selected as 0.1 and 0.5 of the maximum probability density, respectively. Our atomistic calculation shows that

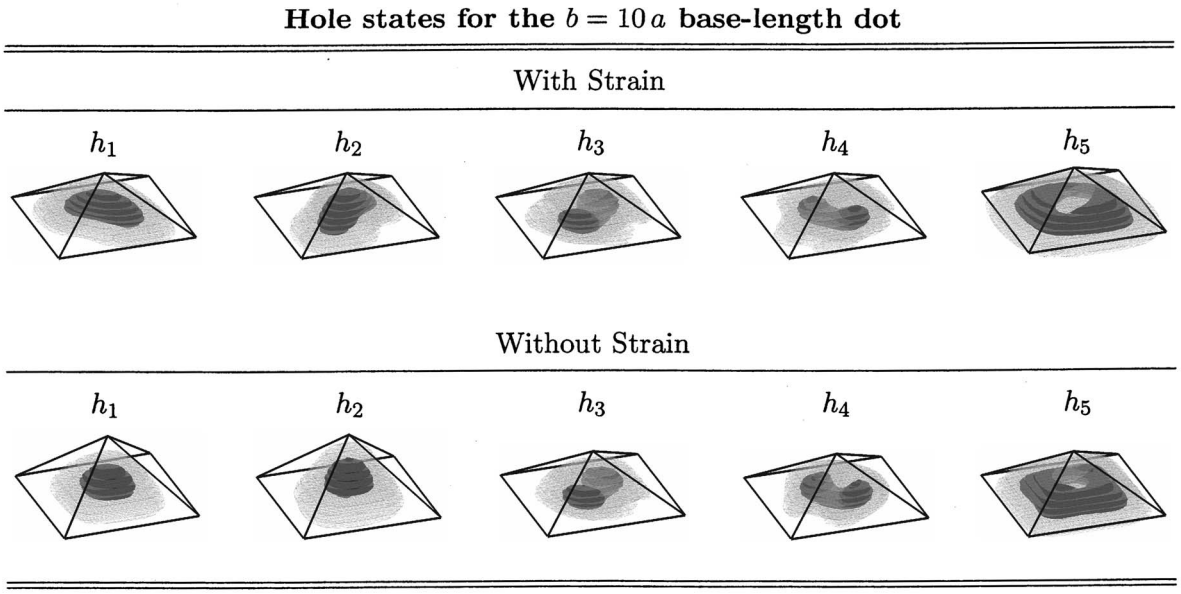

FIG. 6. Isosurfaces plots of the squared hole wave functions with and without strain for the embedded $b=10a$ pyramidal QD. See the caption of Fig. 5 for more details.

the hole states cannot be classified by s-like (h_1), p-like (h_2 and h_3), or d-like (h_5) shape according to their nodal structures. With and without strain the hole states underly a strong band mixing. So the calculated hole states show no nodal structures. Therefore the assumption of a single heavy-hole valence band for the description of the bound hole states in a EQD even qualitatively yields incorrect results. In contrast to quantum well systems, the light-hole and heavy-hole bands are strongly mixed in a EQD. This result is in good agreement with other multiband approaches.[23–29]

From Fig. 6 we can also estimate the influence of strain on the different hole states. Without strain the states h_1 and h_2 are only slightly elongated along the $[1\bar{1}0]$ and [110] directions, respectively. Due to strain these states are clearly elongated along these directions. The states h_3-h_5 are only slightly affected by strain.

Another interesting result is that strain effects shift the electron states to lower energies and the hole states to higher energies as displayed in Fig. 4. Figure 4 also reveals that the WL ground state for electrons and holes is shifted in a similar way due to strain. We observe that strain decreases the EQD gap $E_{\mathrm{gap}}^{\mathrm{QD}}=E_{e_1}-E_{h_1}$ by about 1.4%, lowering it from the strain-unaffected value 2.12 eV to the value 2.09 eV. For a biaxial compressive strain in a zinc blende structure, the conduction-band minimum of a bulk material is shifted to higher energies while the energy shift of the valence-band maximum depends on the magnitude of the hydrostatic and shear deformation energies.[60] So one would expect that the electron states are shifted to higher energies due to the fact that CdSe is compressively strained in the ZnSe matrix. This is in contradiction to the behavior we observe here. To investigate the influence of the WL states on the one-particle spectrum we use the same model geometry as shown in Fig. 2 but with a considerably smaller WL thickness of only 1 ML. A 1 ML thick WL was also used before by Santoprete *et al.*,[35] Stier *et al.*,[23] and Wang *et al.*[26] for an InAs/GaAs EQD. Figure 7 shows the comparison of the results for a strain-unaffected and a strained pyramidal CdSe EQD with a 1 ML thick WL and a base length of $b=10a$.

On the left-hand side of Fig. 7 the first five electron and hole-state energies for an unstrained EQD are displayed while the right-hand side shows the energies for the strained EQD. For a 1 ML thick WL the lowest electron state is, by strain effects, shifted to higher energies. This is what one would expect for biaxial compression of the bulk material.

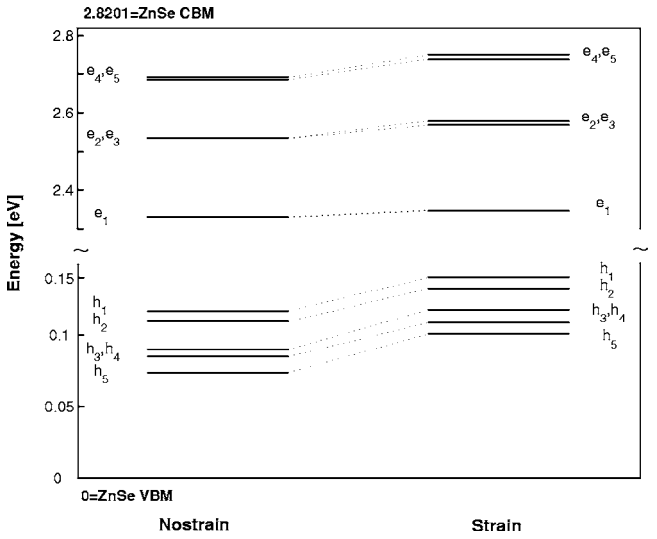

FIG. 7. First five electron and hole state energies for the embedded pyramidal CdSe QD with $b=10a$ and a 1 ML thick WL. On the left-hand side the results for the unstrained EQD are shown while on the right-hand side the results for the strained EQD are displayed. The zero of the energy scale is the bulk ZnSe valence-band maximum (VBM). The energies are compared with the conduction-band minimum (CBM) of the bulk ZnSe.

TABLE III. Energy splittings for electron and hole bound-states in case of different WL thicknesses. The influence of strain effects on the splittings $\Delta_{e_1,e_2}=|E_{e_1}-E_{e_2}|$, $\Delta_{e_2,e_3}=|E_{e_2}-E_{e_3}|$, $\Delta_{h_1,h_2}=|E_{h_1}-E_{h_2}|$, and $\Delta_{h_2,h_3}=|E_{h_2}-E_{h_3}|$ is also displayed. The WL thickness is $1a$ and 1 ML, respectively. The base length of the pyramid is $b=10a$.

WL	$1a$		1 ML	
	No strain	Strain	No strain	Strain
Δ_{e_1,e_2} (meV)	162.8	161.5	204.1	221.2
Δ_{e_2,e_3} (meV)	0.43	7.1	0.5	10.9
Δ_{h_1,h_2} (meV)	5.76	3.7	7.25	7.66
Δ_{h_2,h_3} (meV)	16.36	12.3	19.66	15.11
$E_{\text{gap}}^{\text{QD}}$ (eV)	2.12	2.09	2.21	2.21

Furthermore the splitting of the p-like states e_2 and e_3 is larger compared to the results for a $1a$ thick WL. The splitting Δ_{e_2,e_3}^0 of the unstrained EQD with a $1a$ thick WL is $\Delta_{e_2,e_3}^0=0.43$ meV, whereas for the system with a 1 ML thick WL one has $\Delta_{e_2,e_3}^0=0.5$ meV. So the splitting Δ_{e_2,e_3}^0 is increased by about 16%. With strain-effects, the splitting for the system with 1 ML WL thickness $\Delta_{e_2,e_3}^{\text{strain}}=10.9$ meV is about 54% larger than the splitting in the system with $1a$ WL thickness $\Delta_{e_2,e_3}^{\text{strain}}=7.1$ meV. Also the energy splitting Δ_{e_1,e_2} between the ground state e_1 and the first excited state e_2 is strongly influenced by the WL thickness, namely $\Delta_{e_1,e_2}=162.8$ meV for the unstrained system with $1a$ WL, but $\Delta_{e_1,e_2}=204.1$ meV for a 1 ML WL; with strain effects the splitting Δ_{e_1,e_2} is increased by about 27% if the WL thickness is decreased from $1a$ to 1 ML. The results are summarized in Table III. This effect mainly arises from the fact, that the bound states inside the dot are also coupled to the WL states. For a $1a$ WL the wave functions of the bound states show also a probability density inside the WL. For a thinner WL the leaking of the states into the region of the WL is much less pronounced. In this case, the microscopic structure inside the EQD and also the strain affect are much more important. This explains the larger energy splittings in the case of the 1 ML WL compared to the results for a $1a$ WL. The hole states are influenced in a similar manner. In the case of a 1 ML WL the energy spectrum of the hole states is shifted to higher energies due to the strain effects. This behavior is similar to the behavior obtained from the calculations for a $1a$ WL (Fig. 7). In the 1 ML WL system the energy splittings Δ_{h_1,h_2} and Δ_{h_2,h_3} for the first three hole states are larger than the values we obtain for the system with $1a$ WL. These splittings are also summarized in Table III. The WL thickness also influences the EQD energy gap $E_{\text{gap}}^{\text{QD}}$. For a 1 ML WL the electron states are shifted to higher energies in contrast to the behavior of the hole states (compare Figs. 4 and 7). In the case of the 1 ML WL the gap energy $E_{\text{gap}}^{\text{QD}}$ is only slightly affected by the strain. We observe here that the strain has an opposite effect for electron and hole states: electron states become shallower, approaching the conduction-band edge, while the hole states become deeper, moving away from the valence-band edge.

The knowledge of the single-particle wave functions makes the examination of many-particle effects in EQDs possible. The single particle wave functions can be used for the calculation of Coulomb- and dipole-matrix elements as input parameters. For example the investigation of multiexciton emission spectra,[62] carrier capture and relaxation in semiconductor quantum dot lasers,[63] or a quantum kinetic description of carrier-phonon interactions[64] is possible.

IV. RESULTS FOR CdSe NANOCRYSTALS

A. Geometry and strain

In this section we investigate the single particle states of CdSe nanocrystals within our TB model. These nanostructures are chemically synthesized.[11,12] The nanocrystals are nearly spherical in shape[12,65,66] and the surface is passivated by organic ligands. Due to the flexible surrounding matrix, these nanostructures are nearly unstrained.[66] The size of these nanostructrues is in between 10 and 40 Å in radius.[11,65,67,68]

We model such a chemically synthesized NC as an unstrained, spherical crystallite with perfect surface passivation. The zinc blende structure is assumed for the CdSe nanocrystal. We neglect surface reconstructions[21,39,51] and the fact that the surface coverage with ligands is often not perfect,[69] though these effects can be important especially for very small NCs. However, we concentrate on considerably larger NCs than in the before mentioned references. Therefore, unlike previous TB work we concentrate here on the size and the size dependence of the results obtained for the electronic structure of the NCs. The TB parameters, which describe the coupling between the dot material and the ligand molecules, are chosen to be zero. This corresponds to an infinite potential barrier at the surface and is commonly used because of the larger band gap of the surrounding material.[70] An alternative approach to treat the ligand molecules is discussed by Sapra *et al.* in Ref. 71. The influence of the organic ligands on the electronic structure can also be investigated more realistically within the framework of microscopic descriptions.[39,50,51]

B. Single particle states and comparison with experimental results

We have performed TB calculations for finite, spherical, unstrained NCs of a diameter between 1.82 and 4.85 nm (corresponding to $3-8a$, when $a\approx 6.07$ Å is the CdSe lattice constant of the conventional unit cell). The finite matrix diagonalizations yield both the discrete eigenenergies and the eigenstates. For the largest NCs (of a diameter 4.85 nm) results for the five lowest lying electron and hole eigenstates are shown in Fig. 8 again in the form of an isosurface plot. The lowest lying electronic state e_1 obviously has spherical symmetry and can be classified as a $1s$ state. Correspondingly the second state e_2 has the form of a $2s$ state and the states $e_{3,4}$ are p states, and e_5 is a d-like state. Despite the spherical symmetry of the system this simple classification is no longer possible for the hole states, however. Even the lowest lying hole state h_1 has no full rotational invariance,

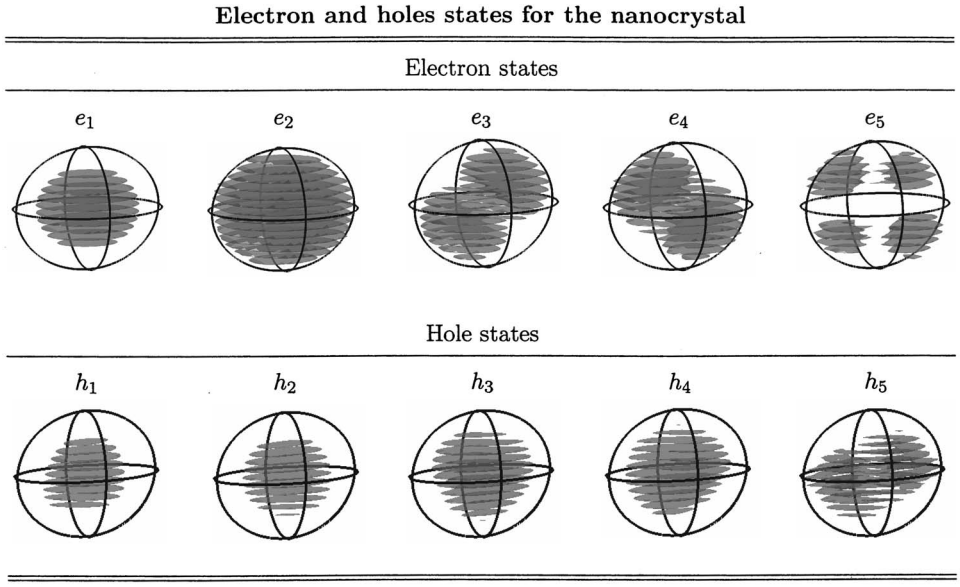

FIG. 8. Isosurfaces (at 30% of the maximum probability density) of the squared electron and hole wave functions of spherical CdSe nanocrystals of diameter d=4.85nm for the five lowest states.

i.e., strictly speaking it cannot be classified as being an s state. This is due to the intermixing of different atomic TB-valence electron states in the NC. Similarly the higher hole states h_2-h_4 cannot clearly be classified as an s- or p-like state. This is an effect, which simple effective mass models cannot account for, but which will have implications in the calculation of matrix elements between these states, which enter selection rules for optical transitions, etc.

In the case of an ideal zinc blende structure as considered here we do not obtain any indications of quasimetallic behavior, i.e., of a nonvanishing (quasicontinuous) spectrum of states at the Fermi energy in contrast to previous work (assuming an ideal wurtzite structure for CdSe nanocrystals).[19,38,39] This is probably due to the fact that this quasimetallic behavior is due to surface states in the case where no passivation and surface reconstruction is taken into account. These surface states are formed by the dangling bonds of unsaturated Se at the NC surface, which cause s states in the band gap region.[38] In our simplified and restricted TB $s_c p_a^3$ basis set these s orbitals at the anions (Se) are not taken into account. Therefore, these surface states, which in reality and in more realistic models are removed (i.e., energetically drawn down and filled) due to passivation and surface reconstruction, do not occur.

The discrete electronic states of semiconductor NCs are experimentally accessible by scanning tunneling microscopy (STM).[65,67,68] The tunnel current I between the metallic tip of the STM and the CdSe nanocrystal, which is, e.g., epitaxially electrodeposited onto a template-stripped gold film, is measured as a function of the bias voltage V. The conductance (dI/dV) is related to the local tunneling density of states. In the dI/dV vs V diagram, several discrete peaks can be observed. These peaks correspond to the addition energies (charging energies) of holes and electrons. The spacing between the various peaks can be attributed to the Coulomb charging (addition spectrum) and/or charge transfer into higher energy levels (excitation spectrum). From these measurements the energy gap $E_{\mathrm{gap}}^{\mathrm{nano}}$ as well as the splitting Δ_{e_1,e_2} between electron ground state e_1 and the first excited state e_2 can be determined.

Alperson *et al.*[68] investigated CdSe nanocrystals with a STM. Here we compare our calculated energy gap $E_{\mathrm{gap}}^{\mathrm{nano}}$, which is given by the difference between the electron, e_1, and hole, h_1, ground state, with measured data from Ref. 68. Figure 9 displays the results for CdSe NCs with diameters in between 1.82 and 4.85 nm. Alperson *et al.*[68] compare the STM results (dashed-dotted line) with optical spectroscopy

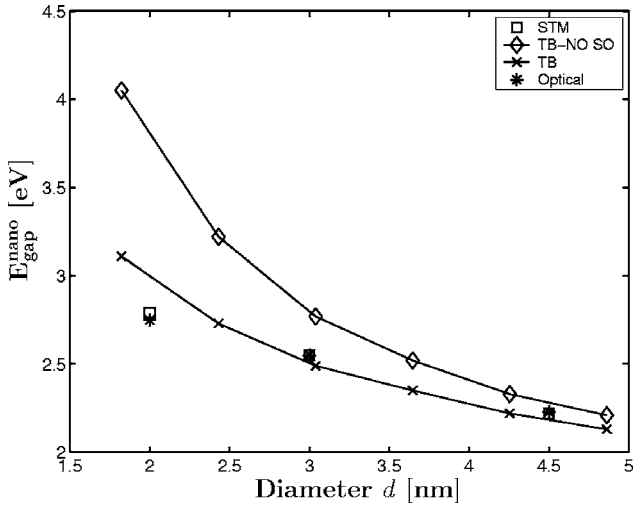

FIG. 9. Energy gap $E_{\mathrm{gap}}^{\mathrm{nano}}$ as a function of the nanocrystal diameter d. Compared are the results from our TB model with (TB) and without (TB-NO SO) spin-orbit coupling, a STM (STM, Ref. 68) and an optical measurement (optical, Ref. 68).

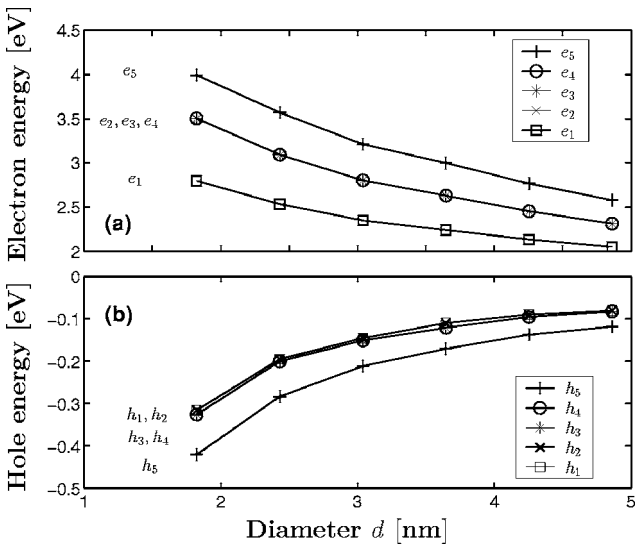

FIG. 10. Electron (a) and hole (b) energies as a function of the nanocrystal diameter d. For electrons (e_1–e_5) and holes (h_1–h_5) the first five eigenvalues are displayed. Each state is twofold degenerated.

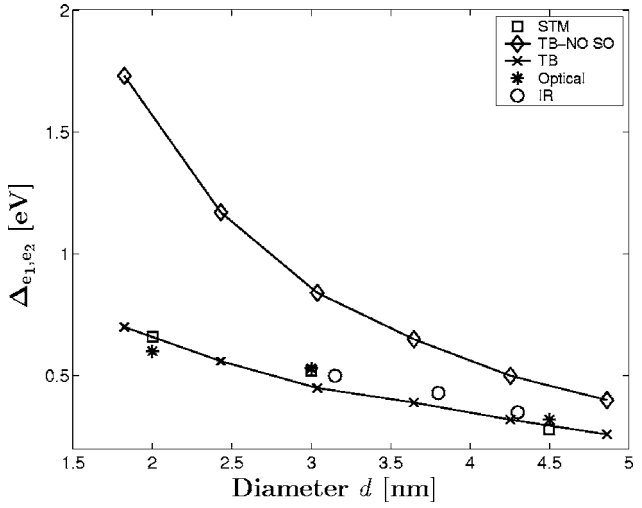

FIG. 11. Splitting $\Delta_{e_1,e_2}=E_{e_2}-E_{e_1}$ between the lowest two electronic states as a function of the nanocrystal diameter d. The results from our TB model, with (TB) and without (TB-NO SO) spin-orbit coupling, and from a STM measurement (STM, Ref. 68) are displayed. Besides this, results from infrared spectroscopy (IR, Ref. 73) and optical methods (optical, Ref. 68) are shown.

measurements (dotted line) from Ekimov *et al.*[72] The overall agreement with the TB results is very good, especially for the larger NCs. Deviations in the case of the small 2 nm NC arise from surface reconstructions[19,21,39] that are neglected here. When the same calculation is done without spin-orbit coupling (TB-NO SO), the energy gap $E_{\mathrm{gap}}^{\mathrm{nano}}$ is always strongly overestimated by the TB model, in particular, for smaller nanocrystals. So the spin-orbit coupling is important for a satisfactory reproduction of the experimental results. For the calculations without spin-orbit coupling, the TB parameters are re-optimized in order to reproduce the characteristic properties (band gap, effective masses) of the bulk material. The re-optimized parameters are given in Table II. Taking into account the electron spin, the lowest electron state e_1 is twofold degenerated and s-like. This is consistent with the experimentally observed doublet[68] in the dI/dV characteristic. The next excited level is (quasi) sixfold degenerated. The spin-orbit coupling splits this into one twofold and one fourfold degenerate state.[34] In the STM measurement Alperson *et al.*[68] observed such a higher multiplicity of the second group of peaks. This behavior has also experimentally[65] and theoretically[34] been observed for InAs nanocrystals. The electron energy spectrum for NCs of different diameters is shown in Fig. 10(a). Here the first five electron states e_1–e_5 are displayed. Note that every state is twofold degenerated due to the spin.

For the hole states the situation is more complicated. Alperson *et al.*[68] observed a high density of states at negative bias. The distinction between addition and excitation peaks is difficult, due to the large number of possibilities and the close proximity between the charging energy and the level spacing. For the holes, we observe that the first two states (h_1,h_2) and (h_3,h_4) are fourfold degenerated. The energy splitting of these states is also very small. These results are consistent to the observations of Alperson *et al.*[68] Figure 10(b) shows the hole energy versus diameter d for the spherical CdSe NCs. Obviously, for all diameters displayed the states h_1-h_4 are almost degenerate, i.e., including spin there is almost an eightfold degeneracy of these states.

Furthermore the calculated splitting $\Delta_{e_1,e_2}=E_{e_2}-E_{e_1}$ between the first two electron states e_1 and e_2 is compared with experimentally observed results for this quantity. Figure 11 shows Δ_{e_1,e_2} as a function of the nanocrystal diameter d. The influence of the spin-orbit coupling on our results is also investigated. We have done the calculations without (TB-NO SO) and with spin orbit-coupling (TB). The results of our TB model for the splitting Δ_{e_1,e_2} are compared with results obtained by STM (Ref. 68) and by optical methods (Optical).[72] This splitting Δ_{e_1,e_2} was independently determined experimentally by Guyot-Sionnest and Hines[73] using infrared spectroscopy (IR). Without spin-orbit coupling the TB model always overestimates the splitting Δ_{e_1,e_2}. Especially for smaller nanocrystals the spin-orbit coupling is very important in describing the electronic structure. With spin-orbit coupling the results of the TB model show good agreement with the experimentally observed results.

V. CONCLUSION

We have applied an empirical $s_c p_a^3$ TB model to the calculation of the electronic properties of II-VI semiconductor EQDs and NCs. Assuming a zinc blende lattice and (per spin direction) one s-like orbital at the cation sites and three p orbitals at the anion sites, the TB parameters for different materials (here ZnSe and CdSe) are determined so that the most essential properties (band gap, effective masses etc.) of the known band structure of the (three-dimensional) bulk materials are well reproduced by the TB band structure. Then a CdSe QD (on top of a two-dimensional, a few atomic layers thick WL) embedded within a ZnSe matrix is modeled by

using the TB parameters of the dot material for those sites occupied by CdSe and the ZnSe TB matrix elements for the remaining sites; suitable averages have to be chosen for intersite matrix elements over and for on-site matrix elements on anion (Se) sites at interfaces between QD and barrier material. Spherical CdSe NCs can be modeled similarly by setting the intersite matrix elements between surface atoms and atoms in the monolayer of surfactant material to zero. The effects of the spin-orbit interaction, the band offsets, and for the EQDs, strain effects are taken into account.

For the EQD systems the numerical diagonalization yields a discrete spectrum of bound electron and hole states localized in the region of the EQD. Energetically these discrete states are below the continuum of the WL states. We have investigated the dependence on the EQD size and find that the number of the bound states and their binding energy increases with increasing dot size, therefore the effective band gap decreases. We have also investigated the dependence of the bound eigenenergies and their degeneracy on strain and on the thickness of the WL. Looking at the states themselves one sees that conduction-band (electron) states can be roughly classified as s-like, p-like, etc. states but the valence-band (hole) states cannot be classified according to such simple (s,p,d) symmetries because they are determined by a mixing between the different (anion) p states. This cannot be accounted for by simple effective mass models but it will be important, for instance, for the calculation of dipole matrix elements between electron and hole states, which determine the selection rules for optical transitions. For the NCs the whole spectrum is discrete, but in spite of the spherical symmetry the hole states do not have the simple s, p, d symmetry but are intermixtures of atomic p orbitals. Even the lowest hole state has no spherical s symmetry but it is fourfold (eightfold including spin) degenerate. The spin-orbit interaction is very important. Including the spin-orbit interaction we obtained nearly perfect agreement with experimental results obtained by STM for the dependence of the band gap and of the splitting of the lowest electronic states on the diameter of the NC.

Compared to (two-band) effective mass[15,22] and multiband $\vec{k}\cdot\vec{p}$ models[23–25] for EQDs our TB model clearly has the advantage of a microscopic, atomistic description. Different atoms and constituents of the nanostructure and their actual positions are considered, and this may lead to a reduction of symmetries (for instance, the C_{2v} symmetry instead of a C_{4v} symmetry). This may automatically lift certain degeneracies and lead automatically to a splitting, for instance, between e_2 and e_3 states, whereas an eight-band $\vec{k}\cdot\vec{p}$ model still yields degenerate e_2 and e_3 states.[25] The effects of inhomogeneous strain can be easily incorporated into a TB model by considering the deviations of the actual atomic positions from the ideal position in the bulk crystal. Only the (empirical) pseudopotential treatment[26–29] may be still superior and more accurate than the TB approach, but in a pseudopotential description a variation of the wave functions within the individual atoms is accounted for and a large number of basis states is required. Therefore, a TB description is simpler and quicker and allows for the investigation of larger nanostructures without loosing information on the essential, microscopic details of the structure. Compared to other TB models of QD structures, we do not consider free-standing, isolated QDs (as in Ref. 42) but we can describe realistic QDs (with a WL) embedded into another barrier material. We show here that a reduced $s_c p_a^3$ basis is already sufficient for a satisfying reproduction of properties such as optical gaps, energy splittings, etc., and their size dependence. Much larger basis sets, namely a sp^3s^* basis[35] or even a $sp^3d^5s^*$ basis[55] were used in previous TB models of EQDs. Our reduced, smaller basis set, of course, leads to computational simplifications and allows for the treatment of larger QDs. Furthermore, we apply our TB model to different materials than investigated previously, namely II-VI CdSe nanostructures, and we investigate also NCs, for which excellent agreement with experimental STM results could be demonstrated.

In the future further applications of our TB model for embedded semiconductor QDs and NCs are planned. Of course applications to QDs of other materials, for instance, nitride systems, and other (e.g., wurtzite) crystal structures are possible. Furthermore, EQDs of other shape and size (dome-shaped, lens-shaped, truncated cones, etc.) or two coupled QDs or free-standing (capped and uncapped) QDs can be investigated. A combination with *ab initio* calculations is also possible by determining the TB parameters from a first-principles band-structure calculation of the bulk material. Furthermore the influence of surface reconstructions and the surfactant material on the results for NCs should be investigated. Especially for small NCs these effects are important. Finally matrix elements of certain observables like dipole matrix elements between the calculated QD electron and hole states can be determined, which are important for selection rules and the optical properties of these systems.

ACKNOWLEDGMENTS

This work has been supported by a grant from the Deutsche Forschungsgemeinschaft No. Cz-31/14-1,2 and by a grant for CPU time from the John von Neumann Institute for Computing at the Forschungszentrum Jülich.

[1] U. Woggon, *Optical Properties of Semiconductor Quantum Dots* (Springer, Berlin, 1997).

[2] P. Michler, *Single Quantum Dots: Fundamentals, Applications, and New Concepts*, Topics in Applied Physics, Vol. 90 (Springer, Berlin, 2000).

[3] A. Passaseo, R. Rinaldi, M. Longo, S. Antonaci, A. L. Convertino, R. Cingolani, A. Taurino, and M. Catalano, J. Appl. Phys. **89**, 4341 (2001).

[4] M. Grundmann, *Nano-Optoelectronics: Concepts, Physics and Devices* (Springer, Berlin, 2002).

[5] P. Michler, A. Kiraz, C. Becher, W. V. Schoenfeld, P. M. Petroff, L. Zhang, E. Hu, and A. Imamoglu, Science **290**, 2282 (2000).
[6] X. Li, Y. Wu, D. Steel, D. Gammon, T. H. Stievater, D. S. Katzer, D. Park, C. Piermarocchi, and L. J. Sham, Science **301**, 809 (2003).
[7] W. G. van der Wiel, S. D. Franceschi, J. M. Elzerman, T. Fujisawa, S. Tarucha, and L. P. Kouwenhoven, Rev. Mod. Phys. **75**, 1 (2003).
[8] J. L. Merz, S. Lee, and J. K. Furdyna, J. Cryst. Growth **184**, 228 (1998).
[9] Y. Yang, D. Z. Shen, J. Y. Zhang, X. W. Fan, B. S. Li, Y. M. Lu, Y. C. Liu, and Y. N. Liu, J. Cryst. Growth **233**, 785 (2001).
[10] B. P. Zhang, D. D. Manh, K. Wakatsuki, and Y. Segawa, J. Cryst. Growth **227**, 645 (2001).
[11] B. S. Kim, M. A. Islam, L. E. Brus, and I. P. Herman, J. Appl. Phys. **89**, 8127 (2001).
[12] A. A. Guzelian, U. Banin, A. V. Kadavanich, X. Peng, and A. P. Alivisatos, Appl. Phys. Lett. **69**, 1432 (1996).
[13] L. Manna, E. C. Scher, and A. P. Alivisatos, J. Am. Chem. Soc. **122**, 12700 (2000).
[14] C. B. Murray, S. Sun, W. Gaschler, H. Doyle, T. A. Betley, and C. R. Kagan, IBM J. Res. Dev. **45**, 47 (2001).
[15] A. Wojs, P. Hawrylak, S. Fafard, and L. Jacak, Phys. Rev. B **54**, 5604 (1996).
[16] P. W. Fry, I. E. Itskevich, D. J. Mowbray, M. S. Skolnick, J. J. Finley, J. A. Barker, E. P. O'Reilly, L. R. Wilson, I. A. Larkin, P. A. Maksym *et al.*, Phys. Rev. Lett. **84**, 733 (2000).
[17] S. Ruvimov, P. Werner, K. Scheerschmidt, U. Gösele, J. Heydenreich, U. Richter, N. N. Ledentsov, M. Grundmann, D. Bimberg, V. M. Ustinov, A. Yu. Egorov, P. S. Kop'ev, and Zh. I. Alferov, Phys. Rev. B **51**, 14766 (1995).
[18] J. Shumway, A. J. Williamson, A. Zunger, A. Passaseo, M. DeGiorgi, R. Cingolani, M. Catalano, and P. Crozier, Phys. Rev. B **64**, 125302 (2001).
[19] A. Puzder, A. J. Williamson, F. Gygi, and G. Galli, Phys. Rev. Lett. **92**, 217401 (2004).
[20] P. Sarkar and M. Springborg, Phys. Rev. B **68**, 235409 (2003).
[21] P. Deglmann, R. Ahlrichs, and K. Tsereteli, J. Chem. Phys. **116**, 1585 (2002).
[22] M. Grundmann, O. Stier, and D. Bimberg, Phys. Rev. B **52**, 11969 (1995).
[23] O. Stier, M. Grundmann, and D. Bimberg, Phys. Rev. B **59**, 5688 (1998).
[24] V. A. Fonoberov and A. A. Baladin, J. Appl. Phys. **94**, 7178 (2003).
[25] C. Pryor, Phys. Rev. B **57**, 7190 (1998).
[26] L.-W. Wang, J. Kim, and A. Zunger, Phys. Rev. B **59**, 5678 (1999).
[27] L. W. Wang, A. J. Williamson, A. Zunger, H. Jiang, and J. Singh, Appl. Phys. Lett. **76**, 339 (2000).
[28] A. J. Williamson, L. W. Wang, and A. Zunger, Phys. Rev. B **62**, 12963 (2000).
[29] J. Kim, L. W. Wang, and A. Zunger, Phys. Rev. B **57**, R9408 (1998).
[30] T. Saito and Y. Arakawa, Physica E (Amsterdam) **15**, 169 (2002).
[31] S. Lee, L. Jönsson, J. W. Wilkins, G. W. Bryant, and G. Klimeck, Phys. Rev. B **63**, 195318 (2001).
[32] S. Lee, J. Kim, L. Jönsson, J. W. Wilkins, G. W. Bryant, and G. Klimeck, Phys. Rev. B **66**, 235307 (2002).
[33] G. Allan, Y. M. Niquet, and C. Delerue, Appl. Phys. Lett. **77**, 639 (2000).
[34] Y. M. Niquet, C. Delerue, M. Lannoo, and G. Allan, Phys. Rev. B **64**, 113305 (2001).
[35] R. Santoprete, B. Koiller, R. B. Capaz, P. Kratzer, Q. K. K. Liu, and M. Scheffler, Phys. Rev. B **68**, 235311 (2003).
[36] N. A. Hill and K. B. Whaley, J. Chem. Phys. **100**, 2831 (1994).
[37] K. Leung, S. Pokrant, and K. B. Whaley, Phys. Rev. B **57**, 12291 (1998).
[38] K. Leung and K. B. Whaley, J. Chem. Phys. **100**, 11012 (1999).
[39] S. Pokrant and K. B. Whaley, Eur. Phys. J. D **6**, 255 (1999).
[40] J. Schrier and K. B. Whaley, Phys. Rev. B **67**, 235301 (2003).
[41] S. Lee, O. L. Lazarenkova, P. von Allmen, F. Oyafuso, and G. Klimeck, Phys. Rev. B **70**, 125307 (2004).
[42] T. Saito, J. N. Schulman, and Y. Arakawa, Phys. Rev. B **57**, 13016 (1998).
[43] Y. D. Kim, M. V. Klein, S. F. Ren, Y. C. Chang, H. Luo, N. Samarth, and J. K. Furdyna, Phys. Rev. B **49**, 7262 (1994).
[44] H. W. Hölscher, A. Nöthe, and C. Uihlein, Phys. Rev. B **31**, 2379 (1985).
[45] V. Pellegrini, R. Atanasov, A. Tredicucci, F. Beltram, C. Amzulini, L. Sorba, L. Vanzetti, and A. Franciosi, Phys. Rev. B **51**, 5171 (1995).
[46] H. Dierks and G. Czycholl, J. Cryst. Growth **185**, 877 (1998).
[47] D. J. Chadi, Phys. Rev. B **16**, 790 (1977).
[48] J. C. Slater and G. F. Koster, Phys. Rev. **94**, 1498 (1954).
[49] M. L. Cohen and J. R. Chelikowski, *Electronic Structure and Optical Properties of Semiconductors*, Springer Series in Solid-State Sciences Vol. 75, 2nd ed. (Springer, Berlin, 1989).
[50] E. Rabani, J. Chem. Phys. **115**, 2361 (2003).
[51] A. Puzder, A. J. Williams, N. Zaitseva, G. Galli, L. Manna, and A. Alivisatos, Phys. Educ. **4**, 2361 (2003).
[52] E. Kurtz, M. Schmidt, M. Baldauf, S. Wachter, M. Grün, H. Kalt, and C. Klingshirn, Appl. Phys. Lett. **79**, 1118 (2001).
[53] S. Lakes, T. Reisinger, B. Hahn, C. Meier, M. Meier, and W. Gebhardt, J. Cryst. Growth **159**, 480 (1996).
[54] T. B. Boykin, G. Klimeck, R. C. Bowen, and F. Oyafuso, Phys. Rev. B **66**, 125207 (2002).
[55] J. M. Jancu, R. Scholz, F. Beltram, and F. Bassani, Phys. Rev. B **57**, 6493 (1998).
[56] S. Froyen and W. A. Harrison, Phys. Rev. B **20**, 2420 (1979).
[57] S. Sapra, N. Shanthi, and D. D. Sarma, Phys. Rev. B **66**, 205202 (2002).
[58] D. Bertho, D. Boiron, A. Simon, C. Jouanin, and C. Priester, Phys. Rev. B **44**, 6118 (1991).
[59] L.-W. Wang and A. Zunger, J. Chem. Phys. **100**, 2394 (1994).
[60] S. L. Chuang, *Physics of Optoelectronic Devices* (Wiley-Interscience, New York, 1995).
[61] C. Pryor, J. Kim, L. W. Wang, A. J. Williamson, and A. Zunger, Appl. Phys. Lett. **72**, 2011 (1998).
[62] N. Baer, P. Gartner, and F. Jahnke, Eur. Phys. J. B **42**, 231 (2004).
[63] T. R. Nielsen, P. Gartner, and F. Jahnke, Phys. Rev. B **69**, 235314 (2004).
[64] J. Seebeck, T. R. Nielsen, P. Gartner, and F. Jahnke, Phys. Rev. B **71**, 125327 (2005).
[65] U. Banin, C. YunWei, D. Katz, and O. Millo, Nature (London) **400**, 542 (1999).
[66] A. P. Alivisatos, Science **271**, 933 (1996).
[67] U. Banin, C. J. Lee, A. A. Guzelian, A. V. Kadavanich, A. P. Alivisatos, W. Jaskolski, G. W. Bryant, A. L. Efros, and M.

Rosen, J. Chem. Phys. **109**, 2306 (1998).
[68] B. Alperson, I. Rubinstein, G. Hodes, D. Porath, and O. Millo, Appl. Phys. Lett. **75**, 1751 (1999).
[69] J. Taylor, T. Kippeny, and S. J. Rosenthal, J. Cluster Sci. **12**, 571 (2002).
[70] P. E. Lippens and M. Lannoo, Phys. Rev. B **39**, 10935 (1989).
[71] S. Sapra and D. D. Sarma, Phys. Rev. B **69**, 125304 (2004).
[72] A. I. Ekimov, F. Hache, M. C. Schanne-Klein, D. Ricard, C. Flytzanis, I. A. Kudryavtsev, T. V. Yazeva, A. V. Rodina, and A. L. Efros, J. Opt. Soc. Am. B **10**, 100 (1993).
[73] P. Guyot-Sionnest and M. A. Hines, Appl. Phys. Lett. **72**, 686 (1998).